Front. Earth Sci. 2018, 12(4): 862–876
https://doi.org/10.1007/s11707-018-0722-z

RESEARCH ARTICLE

Distribution of glycerol ethers in Turpan soils: implications for use of GDGT-based proxies in hot and dry regions

Jingjie ZANG[1], Yanyan LEI[2], Huan YANG (✉)[1]

1 State Key Laboratory of Biogeology and Environmental Geology, School of Earth Sciences, China University of Geosciences, Wuhan 430074, China
2 Department of Geology and Environmental Science, University of Pittsburgh, Pittsburgh, PA 15260, USA

Abstract Proxies based on glycerol dialkyl glycerol tetraethers (GDGTs), a suite of membrane lipids occurring ubiquitously in soils, have generated increasing interest in quantitative paleo-environmental reconstruction. Hot and dry climates are likely to have occurred in the geological past; however, the limitations and applicability of these proxies to hot and dry environments are still unknown. In this study, we analyzed the GDGT distribution in the Turpan (TRP) basin of China, where the highest soil temperature can be approximately 70°C, and the mean annual precipitation (MAP) is 15.3 mm. We compared GDGT-based proxies among TRP soils, Nanyang (NY) soils, and Kunming (KM) soils; these three sites exhibit similar mean annual air temperature (MAAT) albeit contrasting temperature seasonality and MAP. Archaeal isoprenoidal GDGTs (isoGDGTs) dominate over bacterial branched GDGTs (brGDGTs) in most TRP soils; this is a characteristic GDGT distribution pattern for soils from dry regions globally. Another feature is the anomalously high GDGT-0/crenarchaeol ratio, which is generally attributed to the contribution of anaerobic methanogenic archaea by previous studies; however, these anaerobic archaea are unlikely to be highly abundant in the dry TRP soils, indicating that certain uncultured halophilic Euryarchaeota are likely to produce a significant amount of GDGT-0 that finally results in a high GDGT-0/Cren ratio. The changes in the salinity of the TRP soils appear to be an important factor affecting the MBT'_{5ME} and the relative abundance of 6- vs. 5-methyl pentamethylated brGDGTs ($IR_{IIa'}$). This is likely to introduce certain scatters in the correlations between MBT'_{5ME} and MAAT and that between $IR_{IIa'}$ and pH determined at the global scale. A comparison of the MBT'_{5ME}-inferred temperature between TRP, NY, and KM soils does not indicate a significant bias toward summer temperature, indicating that brGDGT paleothermometers in soils could reflect the MAAT.

Keywords GDGTs, Turpan soils, semi-arid and arid areas, salinity, MBT'_{5ME}

1 Introduction

Quaternary environmental reconstruction has become a subject of increasing interest because it can provide a historic baseline for projecting future climate change. During the last few decades, a number of biological (Willard et al., 2001; Lu et al., 2006; Wu et al., 2007; Jiang et al., 2011), geochemical (Thornton and McManus, 1994; Wang et al., 2008; Miranda et al., 2009), and geophysical proxies (Heller and Liu, 1982; Balsam et al., 2011; Újvári et al., 2016) have been developed for paleo-environmental reconstruction in a variety of archives including marine and lake sediments (Zielinski and Gersonde, 1997; Leng and Marshall, 2004), stalagmites (Wang et al., 2008), peat (Pendall et al., 2001; Huang et al., 2015), loess-paleosols (Peterse et al., 2011), as well as ice cores (Kang et al., 2015). However, each proxy has its limitations, particularly when applied to terrestrial environments where a large spatial heterogeneity is present. Therefore, testing the applicability of these proxies to different environments is a fundamental requirement for improving our understanding of their underlying mechanisms.

Microorganisms respond sensitively to ambient environmental change, and the shifts in microbial community and membrane lipid compositions have been considered to be reasonable recorders of temperature changes (Brassell et al., 1986; Schouten et al., 2013). Glycerol dialkyl glycerol tetraethers (GDGTs), derived from both archaea and bacteria, are a suite of lipids that occur widely in soils, peat-bogs, lakes, oceans, hot springs, and stalagmites (Pearson et al., 2004, 2008; Weijers et al., 2006a; Schouten

Received October 8, 2017; accepted June 8, 2018

E-mail: yhsailing@163.com

et al., 2013; De Jonge et al., 2014a; Sinninghe Damsté et al., 2014; Yang et al., 2014, 2015a, 2016). They can be classified into two groups, archaeal isoprenoidal GDGTs (isoGDGTs) and bacterial branched GDGTs (brGDGTs), based on the stereochemistry of glycerol and the structures of alkyl chains (Weijers et al., 2006b) (Fig. 1). IsoGDGTs are composed of isoprenoidal alkyl chains bound to two glycerol backbones via ether bonds, whereas brGDGTs consist of two glycerols and branched alkyl chains with one to three methyl moieties and up to one cyclopentyl moiety. The number of methyls in the branched alkyl chains of brGDGTs, quantified by MBT or MBT' (methylation index of branched tetraethers), exhibits a significant correlation with the mean annual air temperature (MAAT) and soil pH, whereas the number of cyclopentyl moieties of brGDGTs, quantified by CBT (cyclization ratio of branched tetraethers), correlates only with the pH (Weijers et al., 2007; Peterse et al., 2012). The combination of MBT(MBT')/CBT can be used as a proxy for paleo-temperature reconstruction (Peterse et al., 2011; Pancost et al., 2013; Kemp et al., 2014).

Optimized chromatography methodologies enabled the separation of 5- and 6-methyl brGDGTs, two groups of isomers differing only in the methyl position of the alkyl chains (De Jonge et al., 2013). De Jonge et al. (2014a) observed a close relationship between the fractional abundances of 6-methylated brGDGTs and the pH of soils worldwide. In semi-arid and arid regions, the high abundance of 6-methylated brGDGTs can cause the underestimation of MBT'/CBT-derived temperature (De Jonge et al., 2014a). Subsequent to the exclusion of 6-methyl brGDGTs from the MBT' calculation, the correlation between MBT'_{5ME} and MAAT in soils was notably improved (De Jonge et al., 2014a; Yang et al., 2015a). MBT appears to be regulated by water availability rather than by temperature in semi-arid and arid regions (Menges et al., 2014). This is further demonstrated by a study of a soil transect with a soil moisture gradient, which reveals that soil moisture exerts a direct impact on the MBT' and the distribution of 6-methyl brGDGTs (Dang et al., 2016).

Nevertheless, most of these studies with respect to the use of isoGDGTs and brGDGTs focused on soils from relatively cold and dry regions. The hot and dry environment is characterized by high evaporation and high temperature, which causes an excessively arid environment that is harsh to the survival of microorganisms. The Turpan (TRP) basin in western China is such an extreme area. The performance and applicability of GDGT-based proxies in this hot and dry environment are still unknown. In this study, we investigated the GDGTs in the TRP soil to discuss the response of GDGTs to this excessively hot and dry region and to evaluate the applicability of GDGT-based proxies.

2 Materials and methods

2.1 Sampling

The TRP basin, known as the Land of Fire, is located in the eastern part of Xinjiang Uygur Autonomous Region (Fig. 2). It is surrounded by Bogda Mountain, Karawu Mountain, Tianshan Mountain, and Jiaoloutage Mountain, whose elevations are 3500–4000 m. The TRP basin is a

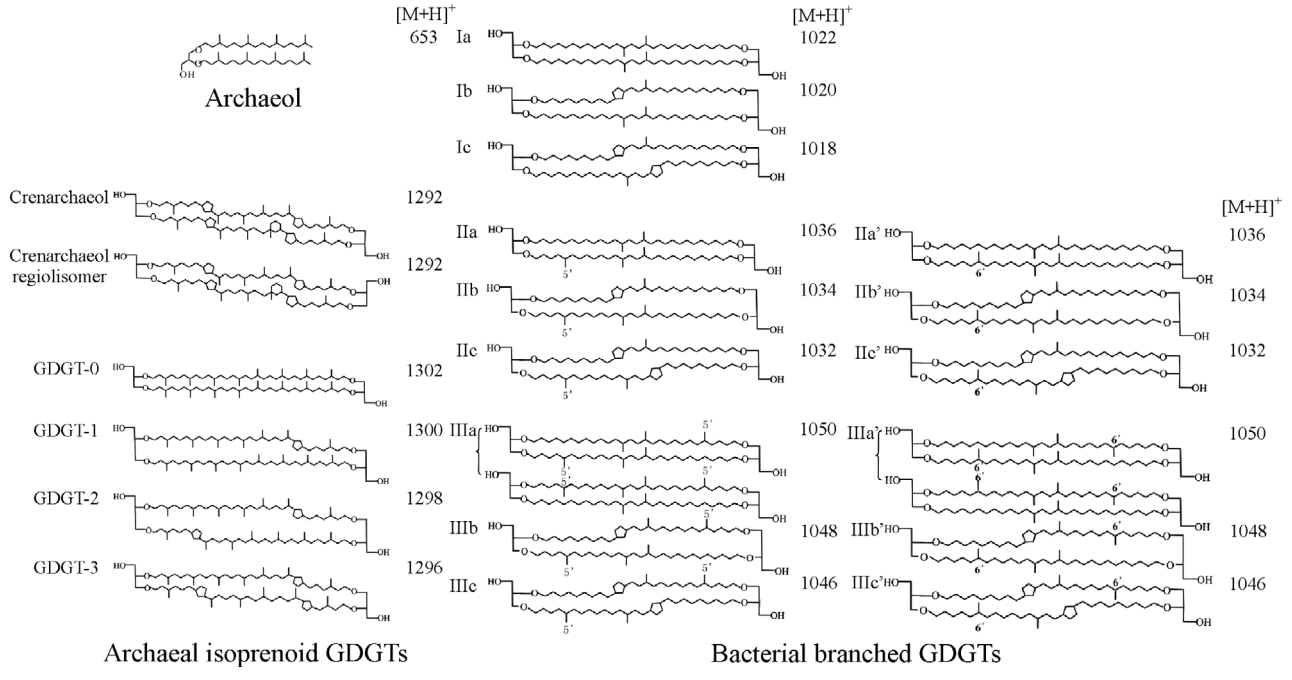

Fig. 1 Structures of archaeol, archaeal isoprenoid GDGTs (isoGDGTs), and bacterial branched GDGTs (brGDGTs).

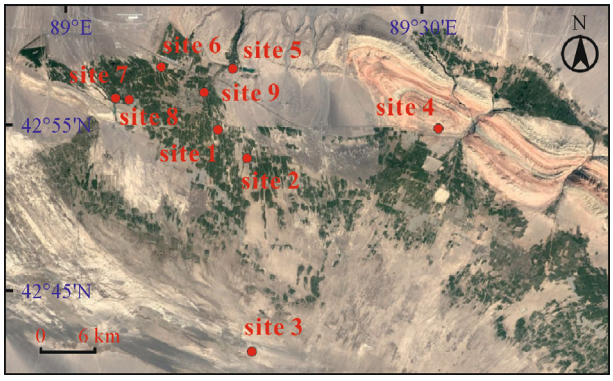

Fig. 2 Sampling sites in TRP basin. The sampling site for each soil sample is listed below: Site 1, TRP-01; Site 2, TRP-02 and TRP-03; Site 3, TRP-04; Site 4, TRP-07 and TRP-08; Site 5, TRP-09, TRP-10, and TRP-11; Site 6, TRP-12, TRP-13, and TRP-14; Site 7, TRP-15 and TRP-16; Site 8, TRP-18, TRP-19, and TRP-20; and Site 9, TRP-21 and TRP-22.

typical example of graben basin with elevation < 500 m and is the lowest inland basin in China. It is subjected to a temperate continental climate with dry and hot summers. The maximum summer air temperatures can reach approximately 50°C, with the ground surface temperature being > 70°C; meanwhile, the mean annual precipitation (MAP) is 15.3 mm (Fig. 3(a) averaged over the 30 y from 1981 to 2010; data from China Meteorological Data Service Center, http://data.cma.cn/). Strong evaporation and minor precipitation result in widespread soil salinization. Vegetation is primarily composed of meadow and steppe varieties. The MAAT for the TRP basin is 15.1°C (Fig. 3(b) averaged over the 30 y from 1981 to 2010, data from China Meteorological Data Service Center, http://data.cma.cn/), which is close to the 30-y MAT record for Nanyang (NY) and Kunming (KM) (15.2°C and 15.5°C, respectively). However, the TRP basin exhibits significantly stronger temperature seasonality than the other two sites. The MAP for NY and KM are 793.3 mm and 979.1 mm, respectively, which are markedly higher than that for TRP.

Samples were collected from nine sites in the TRP basin. In each of the nine sites, one to three soil samples of depths from 0–2 cm were collected in July 2015 (Fig. 2; Table 1). Five subsamples were collected from a 1 m× 1 m square and then combined to form a composite sample. Soil samples were wrapped in aluminum foil and stored in sterile sample bags. They were transported to the laboratory immediately and stored in a refrigerator at −20°C until further analysis.

2.2 Environmental factors

2.2.1 Soil water content

Soil samples were dried in an oven at 40°C for 48 h. SWC (soil water content) was calculated according to the following equation (Yang et al., 2015b):

$$\mathrm{SWC} = (\text{Wet weight} - \text{Dry weight})/\text{Dry weight}. \quad (1)$$

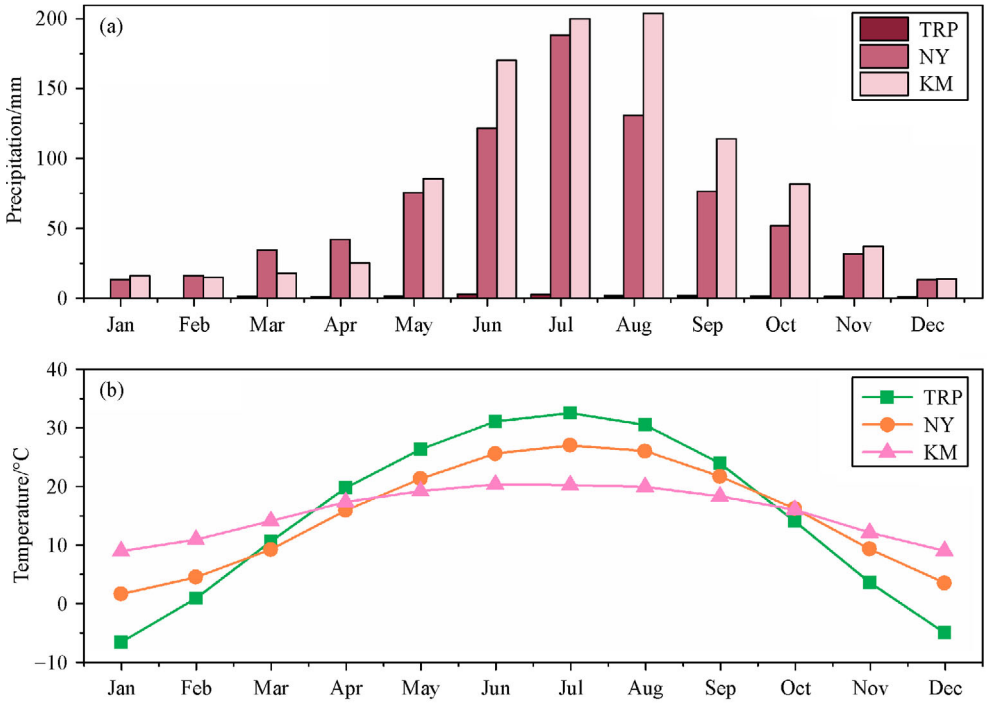

Fig. 3 Mean monthly temperature (a) and precipitation (b) in TRP basin, Nanyang (NY), and Kunming (KM) in China. The mean monthly air temperatures and precipitation were both averaged over the 30 y from 1981 to 2010.

Table 1 Soil-sample information

Sample	Location	Altitude/m	Sampling information
TLF-01	89°13′2″E, 42°54′55″N (site 1)	−17	TLF-01 was collected at a site neighboring a grape-growing region
TLF-02	89°14′51″E, 42°53′26″N (site 2)	−60	TLF-02 and TLF-03 were collected from uncultivated land with sporadically distributed bush. The soils were very dry, hardened, and mixed with gravels
TLF-03	89°14′51″E, 42°53′26″N (site 2)	−60	
TLF-04	89°15′19″E, 42°41′30″N (site 3)	−154	TLF−04 was collected from a barren desert with sporadically distributed bush
TLF-07	89°30′35″E, 42°55′4″N (site 4)	−40	TLF-07 and TLF-08 were collected near the Flaming Mountain. The surface temperature could reach up to 60°C in summer. Soils were very dry without any vegetation
TLF-08	89°30′35″E, 42°55′4″N (site 4)	−40	
TLF-09	89°13′32″E, 42°58′35″N (site 5)	78	TLF-9 and TLF-10 was collected from a woodland and TLF-11 was collected from a farmland
TLF-10	89°13′32″E, 42°58′35″N (site 5)	78	
TLF-11	89°13′32″E, 42°58′35″N (site 5)	78	
TLF-12	89°7′39″E, 42°58′45″N (site 6)	69	TLF-12, TLF-13, and TLF-14 were collected from the Karez paradise
TLF-13	89°7′39″E, 42°58′45″N (site 6)	69	
TLF-14	89°7′39″E, 42°58′45″N (site 6)	69	
TLF-15	89°4′9″E, 42°56′45″N (site 7)	−4	TLF-15 and TLF-16 were collected at a site near the Jiaohe Ruins with trees growing
TLF-16	89°4′9″E, 42°56′45″N (site 7)	−4	
TLF-18	89°4′33″E, 42°56′40″N (site 8)	10	TLF-18, TLF-19, and TLF-20 were collected from a mountain slope
TLF-19	89°4′33″E, 42°56′40″N (site 8)	10	
TLF-20	89°4′33″E, 42°56′40″N (site 8)	10	
TLF-21	89°11′7″E, 42°57′17″N (site 9)	17	TLF-21 and TLF-22 were collected from a mountain slope
TLF-22	89°11′7″E, 42°57′17″N (site 9)	17	

2.2.2 Soil pH

Soil samples were mixed with deionized water in the ratio 1:2.5 (soil (g):water (mL)). The mixture was centrifuged, and the supernatant of each sample was measured three times by using a pH meter with a precision of ±0.01. The average of the three measurements was used as the final pH result (Weijers et al., 2007; Yang et al., 2014).

2.2.3 Salinity

Soil samples and deionized water were mixed in the ratio 1:2.5 (soil (g):water (mL)). The mixture was centrifuged. The cations and anions in the supernatants were analyzed using ion chromatography (ICS600, Thermo Fisher). The cations analyzed included Li^+, Na^+, NH_4^+, K^+, Mg^{2+}, and Ca^{2+}. The anions analyzed included F^-, Cl^-, NO_2^-, SO_4^{2-}, Br^-, NO_3^-, and PO_4^{3-}. The sum of the concentrations of the cations and anions was used to measure the soil salinity.

2.3 Lipid extraction and separation

Samples (10–15 g) were extracted using an accelerated solvent extractor (ASE) with a mixture of dichloromethane and methanol (DCM and MeOH; 9:1, v/v) at 100°C and 7.6×10^6 Pa. The TLE (total lipid extract) was concentrated in a rotary evaporator and then separated into apolar and polar fractions in a flash silica gel column (0.7 cm inside diameter and 1.5 g activated silica gel) with *n*-hexane and a mixture of DCM and MeOH (1:1, v:v), respectively, as eluents. Then, the polar fraction was subjected to saponification with 1 mol/L solution of KOH/MeOH (5% H_2O) (80°C, 2 h). The neutral fraction containing GDGTs were recovered using *n*-hexane (× 5). This fraction was passed through a 0.45 μm PTFE syringe filter and dried under a stream of nitrogen gas.

2.4 GDGT analysis

The GDGTs were analyzed using Agilent 1200 Series high-performance liquid chromatography–atmospheric pressure chemical ionization–mass spectrometry (HPLC-APCI-MS) equipped with autosampler and workstation software. The neutral fraction was spiked with a specified amount of synthesized internal standard (C_{46} GDGT) (Huguet et al., 2006) and re-dissolved in 300 μL of an *n*-hexane–ethyl acetate mixture (84:16, v:v). The injection volume was 10 μL. The separation of 5- and 6-methyl brGDGTs was performed by using two silica columns in tandem (150 mm× 2.1 mm, 1.9 μm, Thermo Finnigan, USA). The *n*-hexane (A) and ethyl acetate (B) were used as the two mobile phases. The GDGTs were eluted isocratically with 84% A and 16% B for the first 5 min. Then, the following elution gradient was used: 84/16 A/B to 82/18 A/B from 5 to 65 min and then to 100% B in 21 min, followed by 100% B for 4 min to wash the column, and then back to 84/16 A/B to balance it for 30 min. A constant flow rate of 0.2 mL/min was used throughout

(Yang et al., 2015a). The MS conditions followed Hopmans et al. (2004). GDGTs and archaeol were detected with single ion monitoring (SIM) at *m/z* 1302, 1300, 1298, 1296, 1292, 1050, 1048, 1046, 1036, 1034, 1032, 1022, 1020, 1018, 653, and 744 (Hopmans et al., 2004). As noted by previous studies, archaeol and GDGTs exhibit distinct responses in the mass spectrometer (Wang et al., 2013). Owing to the absence of a pure archaeol standard in our laboratory, the absolute concentration of archaeol and GDGTs cannot be determined. Therefore, we assumed the response factor among C_{46} GTGT internal standard, archaeol, and GDGTs to be 1:1:1; thus, the final concentration of archaeol and GDGTs can be considered as semi-quantitative.

2.5 Calculation of GDGT proxies

The BIT index was calculated according to the following equation (Hopmans et al., 2004):

$$\mathrm{BIT} = (\mathrm{Ia} + \mathrm{IIa} + \mathrm{IIa'} + \mathrm{IIIa} + \mathrm{IIIa'})/(\mathrm{Ia} + \mathrm{IIa} + \mathrm{IIa'} + \mathrm{IIIa} + \mathrm{IIIa'} + \mathrm{Crenarchaeol}). \quad (2)$$

The CBT (Weijers et al., 2007) and MBT' indices (Peterse et al., 2012) were calculated as follows:

$$\mathrm{CBT} = -\log[(\mathrm{Ib} + \mathrm{IIb} + \mathrm{IIb'})/(\mathrm{Ia} + \mathrm{IIa} + \mathrm{IIa'})], \quad (3)$$

$$\mathrm{MBT'} = (\mathrm{Ia} + \mathrm{Ib} + \mathrm{Ic})/(\mathrm{Ia} + \mathrm{Ib} + \mathrm{Ic} + \mathrm{IIa} + \mathrm{IIa'} + \mathrm{IIb} + \mathrm{IIb'} + \mathrm{IIc} + \mathrm{IIc'} + \mathrm{IIIa} + \mathrm{IIIa'}). \quad (4)$$

The $\mathrm{MBT'_{5ME}}$, $\mathrm{CBT_{5ME}}$, $\mathrm{MBT'_{6ME}}$, and $\mathrm{CBT_{6ME}}$ indices were calculated based on the separated 5- and 6-methyl brGDGTs (De Jonge et al., 2014a; Yang et al., 2015a):

$$\mathrm{MBT'_{5ME}} = (\mathrm{Ia} + \mathrm{Ib} + \mathrm{Ic})/(\mathrm{Ia} + \mathrm{Ib} + \mathrm{Ic} + \mathrm{IIa} + \mathrm{IIb} + \mathrm{IIc} + \mathrm{IIIa}), \quad (5)$$

$$\mathrm{CBT_{5ME}} = -\log[(\mathrm{Ib} + \mathrm{IIb})/(\mathrm{Ia} + \mathrm{IIa})], \quad (6)$$

$$\mathrm{MBT'_{6ME}} = (\mathrm{Ia} + \mathrm{Ib} + \mathrm{Ic})/(\mathrm{Ia} + \mathrm{Ib} + \mathrm{Ic} + \mathrm{IIa'} + \mathrm{IIb'} + \mathrm{IIc'} + \mathrm{IIIa'}), \quad (7)$$

$$\mathrm{CBT_{6ME}} = -\log[(\mathrm{Ib} + \mathrm{IIb'})/(\mathrm{Ia} + \mathrm{IIa'})]. \quad (8)$$

$R_{\mathrm{i/b}}$ was defined as follows (Xie et al., 2012):

$$R_{\mathrm{i/b}} = \sum \mathrm{isoGDGTs} / \sum \mathrm{brGDGTs}. \quad (9)$$

$\mathrm{IR}_{x'}$ was calculated according to the following equation (De Jonge et al., 2014b):

$$\mathrm{IR}_{x'} = x'/(x + x'). \quad (10)$$

Global calibrations for MAAT reconstruction based on $\mathrm{MBT'_{5ME}}$ and fractional abundance were developed by De Jonge et al. (2014a) and were calculated according to the following formulas:

$$\mathrm{MAAT} = 31.45 \times \mathrm{MBT'_{5ME}} - 8.57, \quad (11)$$

$$\mathrm{MAAT_{mr}} = 1.17 + 1.17 \times f(\mathrm{Ia}) + 25.9 \times f(\mathrm{Ib}) + 34.4 \times f(\mathrm{Ic}) - 28.6 \times f(\mathrm{IIa}). \quad (12)$$

2.6 Statistical analysis

The statistical analyses were performed using the SPSS 19.0 software. Significant differences between samples are defined by the Pearson coefficient (p value) < 0.05. We used the Canoco v. 4.5 software to explore the relationships between the GDGT proxies and environmental factors (SWC, pH, and salinity). First, DCA (detrended correspondence analysis) was performed to determine the model that fits the data of this study. Results revealed that the data were suitable for a linear model (the length of gradient in DCA < 3). Then, RDA (redundancy analysis) was used to identify the key environmental control on the GDGT distribution (ter Braak and Smilauer, 2002).

3 Results and discussion

3.1 Distribution of GDGTs and archaeol in hot and dry environment

Both isoGDGTs and brGDGTs were detected in all the TRP soils (Table 2), with the total abundances of isoGDGTs being generally higher than those of brGDGTs. This is consistent with the GDGT distributions in alkaline soils from other semi-arid and arid areas of China (Yang et al., 2014). GDGT-0 and crenarchaeol are the major isoGDGT components (Fig. 4), with concentrations varying from 0.21 to 575.22 ng/g dry wt. soil and from 0.01 to 93.89 ng/g dry wt. soil, respectively. Generally, GDGT-0 exhibits an approximately two-fold higher abundance than crenarchaeol does. Archaeol is found in each soil sample, with the concentration ranging from 1.61 to 44.14 ng/g dry wt. soil. Numerous lines of genetic evidence reveal that halophilic archaea dominate the archaeal community in saline soils (Auguet et al., 2010). The membrane lipids of pure cultures of halophilic archaea are primarily composed of archaeol and extended archaeol (C_{20}–C_{25} dialkyl glycerol diethers) (Schouten et al., 2013). This indicates that halophilic archaea are important constituents of the archaeal community in the TRP soils. The ratio of crenarchaeol to its regioisomer can be used to distinguish the Thaumarchaeota Group I.1a and Group I.1b (Sinninghe Damsté et al., 2012). This ratio varies from 7.5

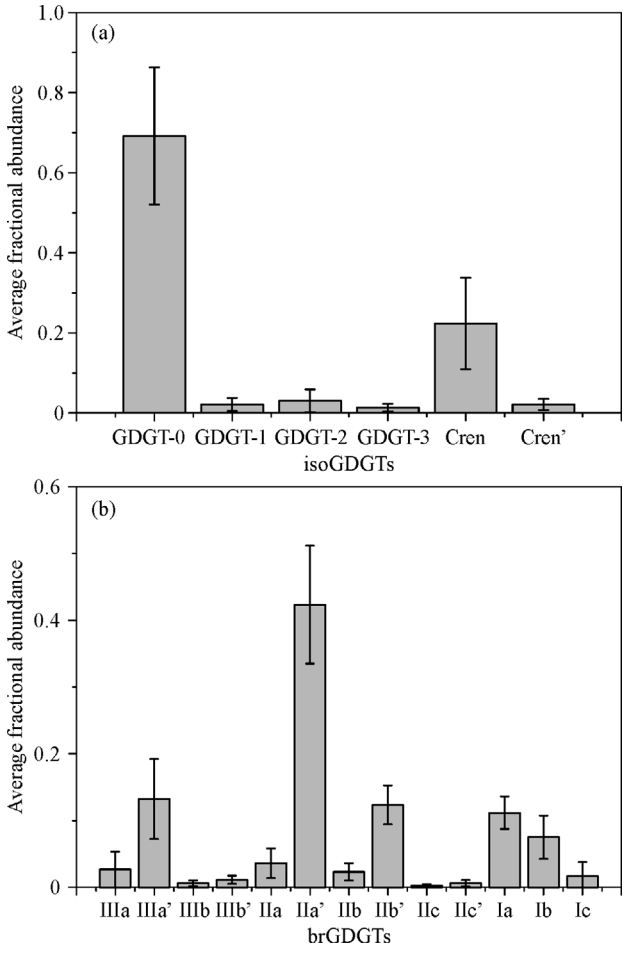

Fig. 4 Average fractional abundances of isoGDGTs (a) and brGDGTs (b) in the TRP soils. The error bars display the range of the fractional abundances of isoGDGTs and brGDGTs.

to 20.7, which is significantly lower than that for the Thaumarchaeota Group I.1a (generally > 50; Sinninghe Damsté et al., 2012). As crenarchaeol is generally more abundant than archaeol is, Thaumarchaeota Group I.1b is likely to be the dominant archaeal group in these soils.

The 6-methyl brGDGTs, including IIIa', IIIb', IIa', IIb', and IIc' (Fig. 4), dominate the brGDGT profile. The concentrations of IIIa' and IIa' range from 0.08 to 25.84 ng/g dry wt. soil and from 0.19 to 63.94 ng/g dry wt. soil, respectively. The 5-methyl brGDGTs are dominated by IIIa and IIa. The concentration of total 5-methyl brGDGTs ranged from 0.06 to 12.37 ng/g wt. soil, whereas that of 6-methyl brGDGTs varies from 0.31 to 116.38 ng/g dry wt. soil. This brGDGT distributional pattern is similar to that for soils from the other arid and semi-arid regions (Dang et al., 2016; Wang et al., 2016).

3.2 Response of microbial GDGTs to excessively dry environment

The excessively low MAP (15.3 mm) results in the development of saline and arid soils in the TRP basin. Therefore, soil moisture is an important limiting factor for the growth of microorganisms in the TRP soils. We compared the GDGT-based proxies among the KM soils, NY soils, and TRP soils to investigate the microbial adaptation strategy in the arid environment. These three sites exhibit similar MAAT, albeit a contrasting MAP. The overall distribution of GDGTs in the TRP soils is different from those in the other two sites. The isoGDGTs dominate over the brGDGTs in the TRP soils, whereas the other two sites exhibit the reverse. This is clearly reflected by the larger $R_{i/b}$ ratios (0.35–8.14, average 2.45; Fig. 5(a)) and the significantly lower BIT values (0.54–0.89, average 0.70; Fig. 5(b)) of the TRP soils compared to those of the other two sites ($R_{i/b}$: 0.01–0.74, average 0.28 for NY; 0.03–0.42, average 0.17 for KM; Fig. 5(a); BIT: 0.50–1, average 0.79 for NY; 0.76–0.99, average 0.92 for KM; Fig. 5(b)). A higher $R_{i/b}$ ratio and a lower BIT value in the arid soils have been conjectured to be associated with a more ventilated and alkaline soil condition that favors the growth of aerobic Thaumarchaeota and inhibits the proliferation of brGDGT-producing bacteria (Yang et al., 2014).

The GDGT-0/Cren ratio of the TRP soils is notably higher than those in the other two sites, wherein this ratio is similar to those of the Chinese soils reported by Yang et al. (2014) (Fig. 6(b)). A high GDGT-0/Cren ratio can be observed also for other saline soils from arid regions in China (Yang et al., 2014). Based on the available knowledge, a GDGT-0/Cren ratio significantly higher than two can only be attributed to the dominance of methanogens or (and) miscellaneous crenarchaeota group (MCG) in the archaeal community (Blaga et al., 2009; Schouten et al., 2013; Besseling et al., 2018). This is because the major membrane lipids for most methanogens and MCG are GDGT-0 and archaeol (Schouten et al., 2013; Besseling et al., 2018). Although a number of sites exhibit GDGT-0/cren > 2 for TRP saline soils, it appears that methanogens are unlikely to dominate in these arid soils (SWC close to zero) because they require anoxic conditions to proliferate. In addition, recent genetic results reveal that methanogens and MCG are limited in arid and saline soils (Valenzuela-Encinas et al., 2008). This contradiction indicates that a few of the halophilic Euryarchaeota that are yet to be characterized are likely to produce abundant GDGT-0, which increases the GDGT-0/Cren ratio in the TRP soils.

The arid climate in the TRP basin also increases the alkalinity of the soils, resulting in the higher soil pH in TRP compared to those of the other two sites (Fig. 7). The $IR_{IIa'}$ value, expressing the relative abundance of 6- vs. 5-methyl pentamethylated brGDGTs, is consistently higher in the TRP soils than in the KM and NY soils (Fig. 5(c)); this is consistent with the perspective that $IR_{IIa'}$ is related to the soil pH in soils globally (De Jonge et al., 2014a; Yang et al., 2015a). As the biological source(s) of 5- and 6-methyl brGDGTs are still unknown, the shift in the

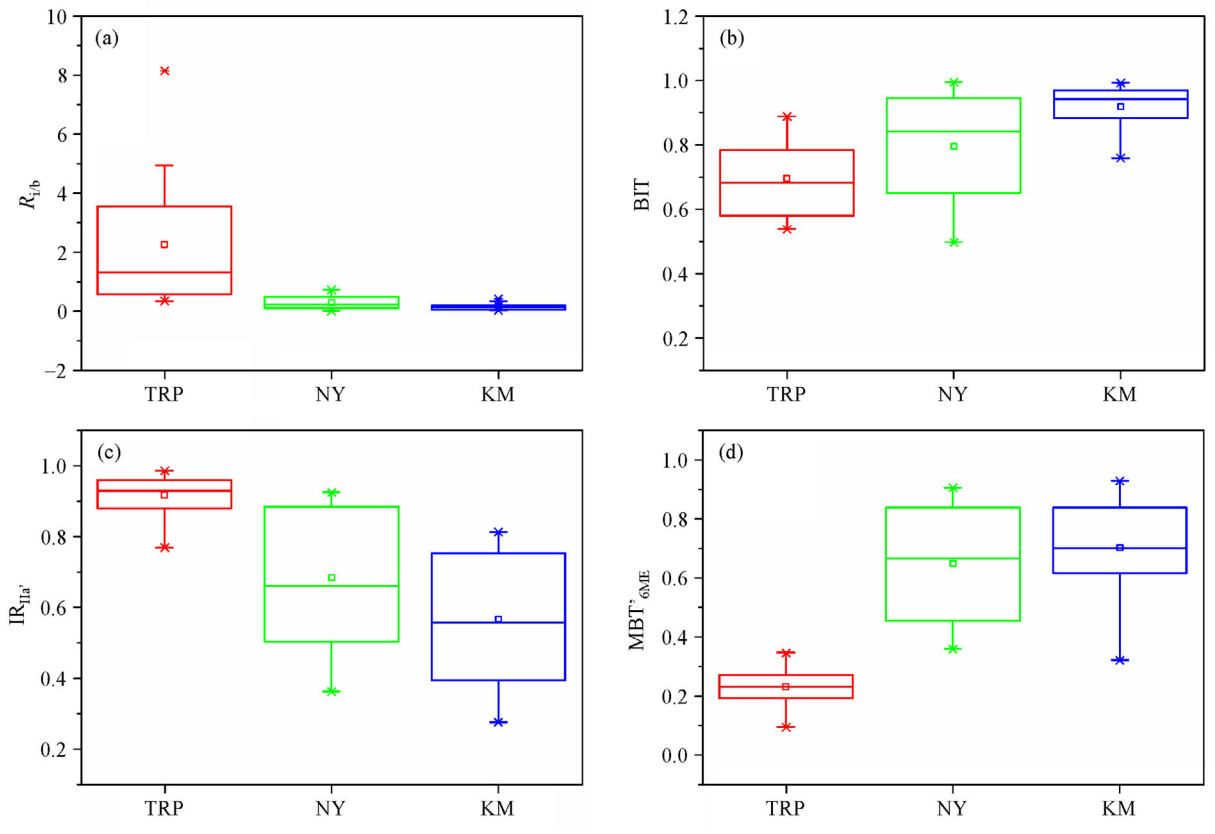

Fig. 5 Box plots showing the range of (a) $R_{i/b}$, (b) BIT, (c) $IR_{IIa'}$, and (d) MBT'$_{6ME}$ in the TRP, NY, and KM soils.

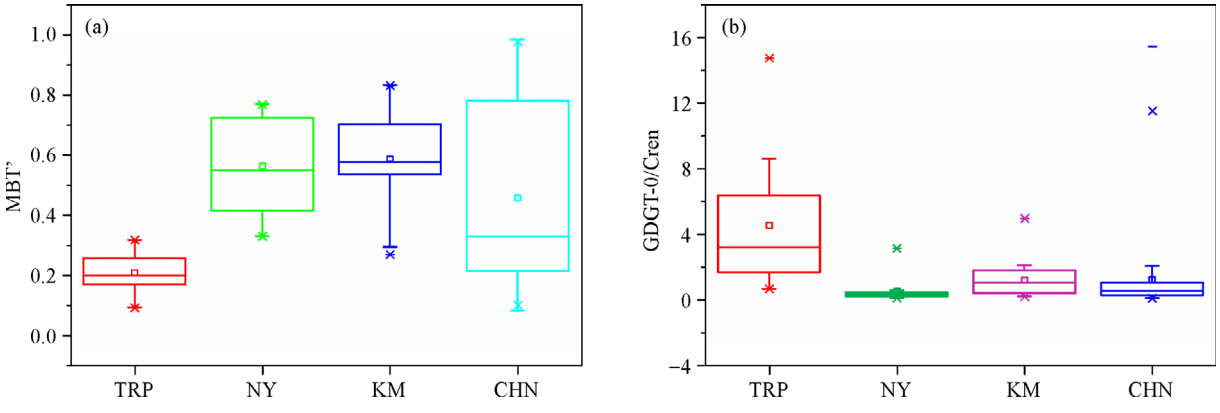

Fig. 6 Box plots showing range of (a) MBT' and (b) GDGT-0/Cren for the TRP, NY, and KM soils and other Chinese soils (CHN) as reported by Yang et al. (2014).

microbial community has been generally invoked to explain the variation of $IR_{IIa'}$ in soils (De Jonge et al., 2014a; Yang et al., 2015a). Another likely explanation is that the source bacteria can change the membrane lipid compositions in order to adapt to the ambient pH change. In addition, the MBT', a measure of the methyl moieties in the brGDGTs, was significantly lower in the TRP soils than in the KM and NY soils irrespective of the fact that the three sites exhibit similar MAAT (Fig. 6(a)). As noted by Dang et al. (2016), the MBT' was primarily related to the MAP when $IR_{6ME} > 0.5$. The IR_{6ME} values in the TRP soils were all higher than 0.5; moreover, the plot of the MBT' for the TRP soils vs. the MAP, extended using the data from northern China (Wang et al., 2016) and global datasets (De Jonge et al., 2014a) with $IR_{6ME} > 0.5$, reveals that MBT' exhibits a strong positive correlation with MAP ($R^2 = 0.68$, $p < 0.05$; Fig. 8(a)). Therefore, precipitation impacts the distribution of brGDGTs in soils from semi-

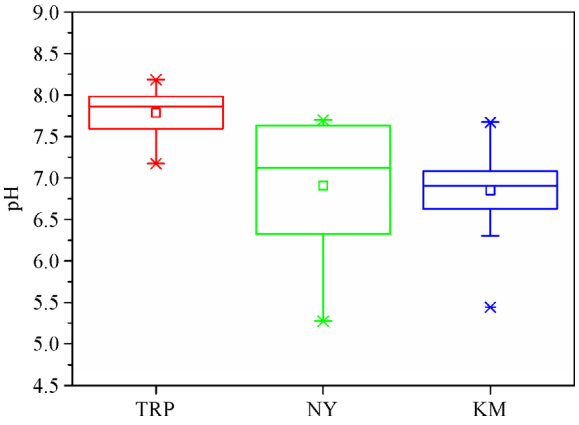

Fig. 7 Box plot showing pH range for TRP, NY, and KM soils.

arid and arid regions. This can be also supported by a soil moisture transect study in the vicinity of the Erhai Lake, where the MBT' decreases as soil aridity increases (Dang et al., 2016). As the brGDGTs are dominated by 6-methyl isomers in the TRP soils, the MBT'$_{6ME}$ values for the TRP basin are also markedly lower than those for the other two sites (Fig. 5(d)). A similar correlation between MBT'$_{6ME}$ and MAP can be observed ($R^2 = 0.65$, $p < 0.05$; Fig. 8(b)), highlighting the feasibility of application of this proxy to reconstruct paleo-precipitation in semi-arid and arid regions. As 6-methyl brGDGTs dominate the brGDGT profile in the TRP soils, MBT' is strongly dependent on the variation of 6-methyl brGDGTs; thus, the variation of MBT' is highly similar to that of MBT'$_{6ME}$. The low MBT'$_{6ME}$ can explain why the global calibration of the MBT'/CBT proxy (Peterse et al., 2012) generally underestimates the temperature in soils from semi-arid and arid regions. The MBT' proxy is related to precipitation rather than temperature and cannot be used to reconstruct temperature in arid soils. The temperature derived from the global MBT'/CBT calibration of Peterse et al. (2012) is between −0.9°C and 9.4°C, which is significantly lower than the actual MAAT (15.1°C).

3.3 Regional environmental control on GDGT-based proxies

As the temperature difference between the sampling sites

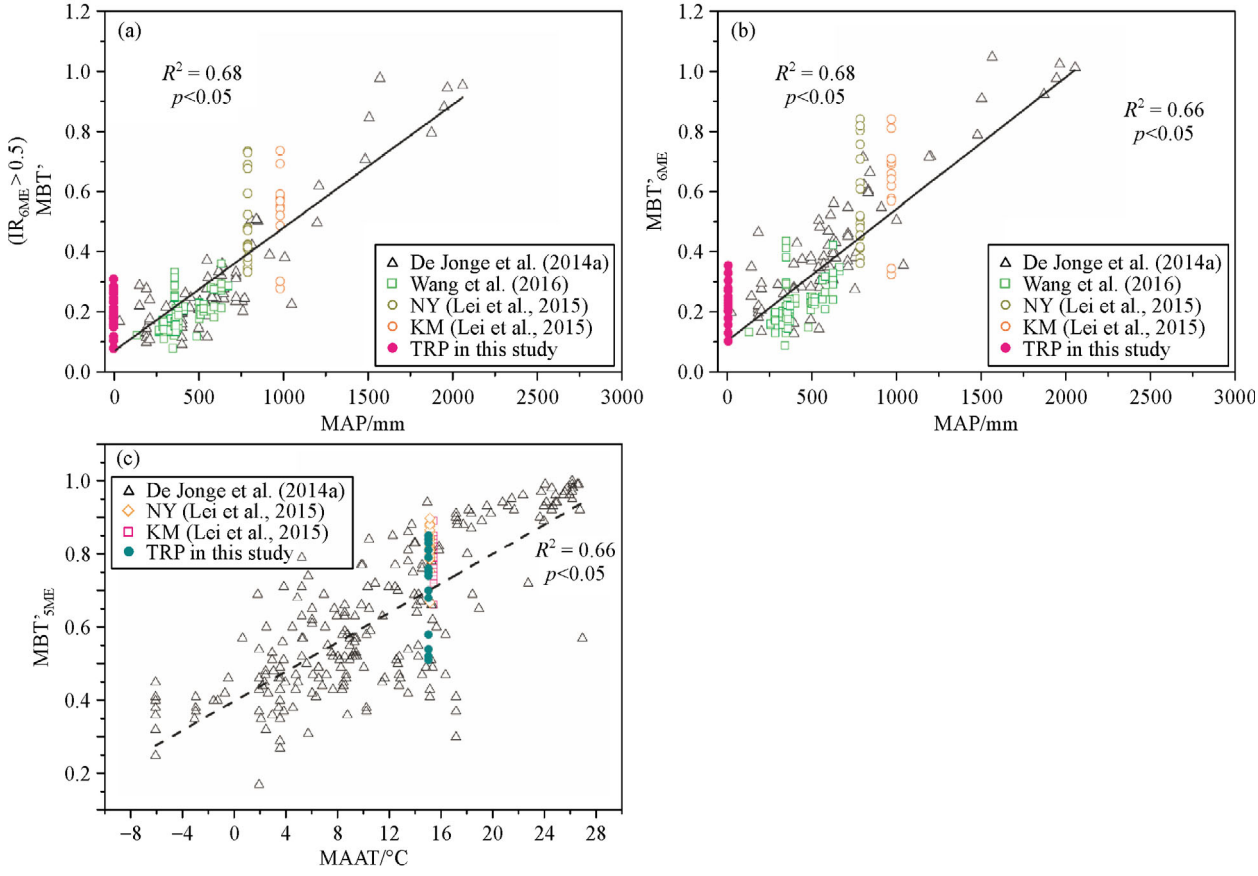

Fig. 8 Scatter plot showing correlation between MBT' and MAP (a), between MBT'$_{6ME}$ and MAP (b), and between MBT'$_{5ME}$ and MAAT (c). Data for global soils (De Jonge et al., 2014a), soils from Northern China (Wang et al., 2016), the NY soils (Lei et al., 2016), the KM soils (Lei et al., 2016), and the TRP soils are compiled here. Here, IR$_{6ME}$ for all the selected data are > 0.5. Two outlier soil samples (Ecuador-19 and Egypt-1; De Jonge et al., 2014a) are excluded from the global soils. Meanwhile, the samples collected from northern China around Da Hinggan Mountains are also excluded from the plot because the soil pH of these soils < 7. The dotted line in (c) exhibits the linear correlation between the MBT'$_{5ME}$ and MAAT of the global soils ($R^2 = 0.66$, $p < 0.05$), as reported by De Jonge et al. (2014a).

in the TRP basin is marginal, we can investigate the likely impact of other environmental controls on the GDGT-based proxies. RDA (Redundancy analysis) was used to determine the environmental control on the GDGT proxies. The two axes explain 14.6% of the variance. The curves for the samples with lower pH and salinity were plotted on the two left quadrants (Fig. 9). In previous studies, MBT and MBT' exhibited positive relationships with MAAT, whereas CBT exhibited a negative correlation with soil pH (Weijers et al., 2007) or SWC (Wang et al., 2014; Dang et al., 2016). However, the RDA plot shows an absence of relationship of MBT' and CBT with pH and SWC in the TRP soils. Rather, soil salinity appears to impact $IR_{IIa'}$ and the fractional abundance of 6-methyl brGDGTs. Thus, the relationships between the GDGT distributions and the environmental variables in the TRP soils are different from those for the other soils.

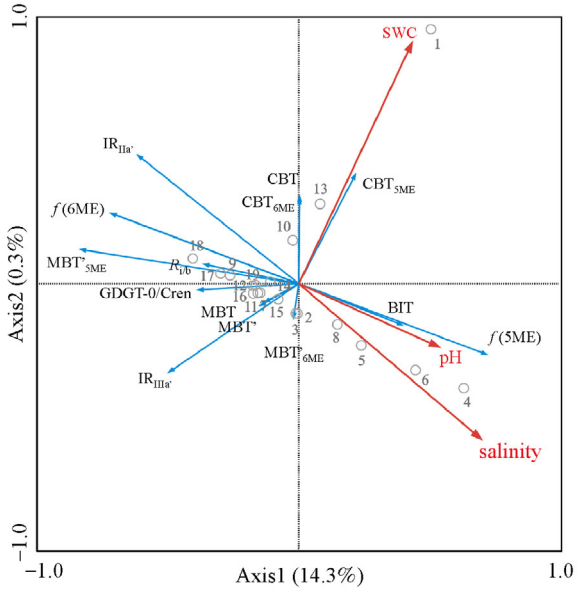

Fig. 9 RDA plots showing relationship between environmental variables and GDGT proxies. The numbers in the plots represent the corresponding samples in the table (Table 1, in the order of TLF-01 to TLF-22).

Most of the GDGT-based proxies in the TRP soils exhibit broad ranges, although the sampling sites were short distances from each other. For example, MBT'_{5ME} varies between 0.51 and 0.85, MBT'_{6ME} varies between 0.09 and 0.35 (Table 3), and CBT varies between 0.17 and 0.82 (Table 3). These three proxies have been determined to be unrelated to either the soil pH or SWC in these soils. Moreover, they have revealed that the soil salinity is likely to be the key factor affecting the brGDGT distribution in these soils. The fractional abundance of 6-methyl brGDGTs, i.e., *f*(6ME), ranges from 0.75 to 0.97 (Table 3); this indicates a negative exponential relationship of *f*(6ME) with salinity ($R^2 = 0.55, p < 0.05$; Fig. 10(b)). $IR_{IIa'}$ ranges from 0.77 to 0.99 (Table 3) and also exhibits a significant negative correlation with salinity ($R^2 = 0.63$, $p < 0.05$; Fig. 10(c)). MBT'_{5ME} spans a broad range, equivalent to a temperature range from 7.6°C to 18.2°C, indicating that factor(s) additional to temperature are likely to affect the MBT'_{5ME} values in excessively arid regions. Soil salinity is observed to be a likely factor causing such a large MBT'_{5ME} range because it exhibits a more or less negative correlation with soil salinity ($R^2 = 0.40$, $p < 0.05$; Fig. 10(d)). The highest soil salinity occurs in the soils without vegetation cover (sites 3 and 4). The high evaporation in these sites results in increased soil salinity. With increased soil salinity, MBT'_{5ME} tends to underestimate the temperature. These results indicate that the change in the soil salinity is likely to introduce a few scatters in the calibration of the MBT'_{5ME} in arid regions, complicating and limiting the worldwide application of the MBT'_{5ME}. However, plotting the MBT'_{5ME} for the TRP soils and global soils (De Jonge et al., 2014a) with respect to the MAAT reveals that the data of the TRP soils are in the vicinity of the fitted line of the global MBT'_{5ME} calibration (Fig. 8(c)). This indicates that the MAAT is the first-order factor regulating the MBT'_{5ME} in excessively dry soils, although the MBT'_{5ME} value appears to be marginally affected by soil salinity.

Similar to brGDGTs, the ratio archaeol/GDGT-0 is significantly correlated with salinity ($R^2 = 0.43$, $p < 0.05$; Fig. 10(a)). This demonstrates the relationship of archaeol with halophilic archaea in these soils (Wang et al., 2013). As large scatters are present in the correlation, the applicability of this proxy to reconstruct paleo-salinity is to be verified. Recently, archaeol has been observed to be produced by Thaumarchaeota, halophilic Euryarchaeota, and methanogens, notwithstanding the fact that its abundance in each archaeal species varies markedly (Pancost et al., 2011; Elling et al., 2017). GDGT-0 also has multiple origins, e.g., Thaumarchaeota (Elling et al., 2017), MCG (Besseling et al., 2018), and methanogens (Blaga et al., 2009; Schouten et al., 2013). This complicated the interpretation of the archaeol/GDGT-0 ratio in the paleo-records.

3.4 Seasonality of GDGT-based temperature proxies

The MAAT for TRP, NY, and KM are 15.1°C, 15.2°C, and 15.5°C, respectively. However, these three sites exhibit contrasting temperature seasonality, with the strongest seasonality occurring in the TRP basin. The monthly average temperature for winter is below 0°C in TRP, whereas they are above 0°C in NY and KM. In contrast, the monthly average temperature for summer in TRP is significantly higher than those of the other two sites (Fig. 3(b)). The brGDGT-based paleo-thermometers, e.g., MBT'/CBT, MBT'_{5ME}, and $MAAT_{mr}$, have been considered for recording the MAAT rather than the seasonal temperature (Weijers et al., 2007; Peterse et al., 2012).

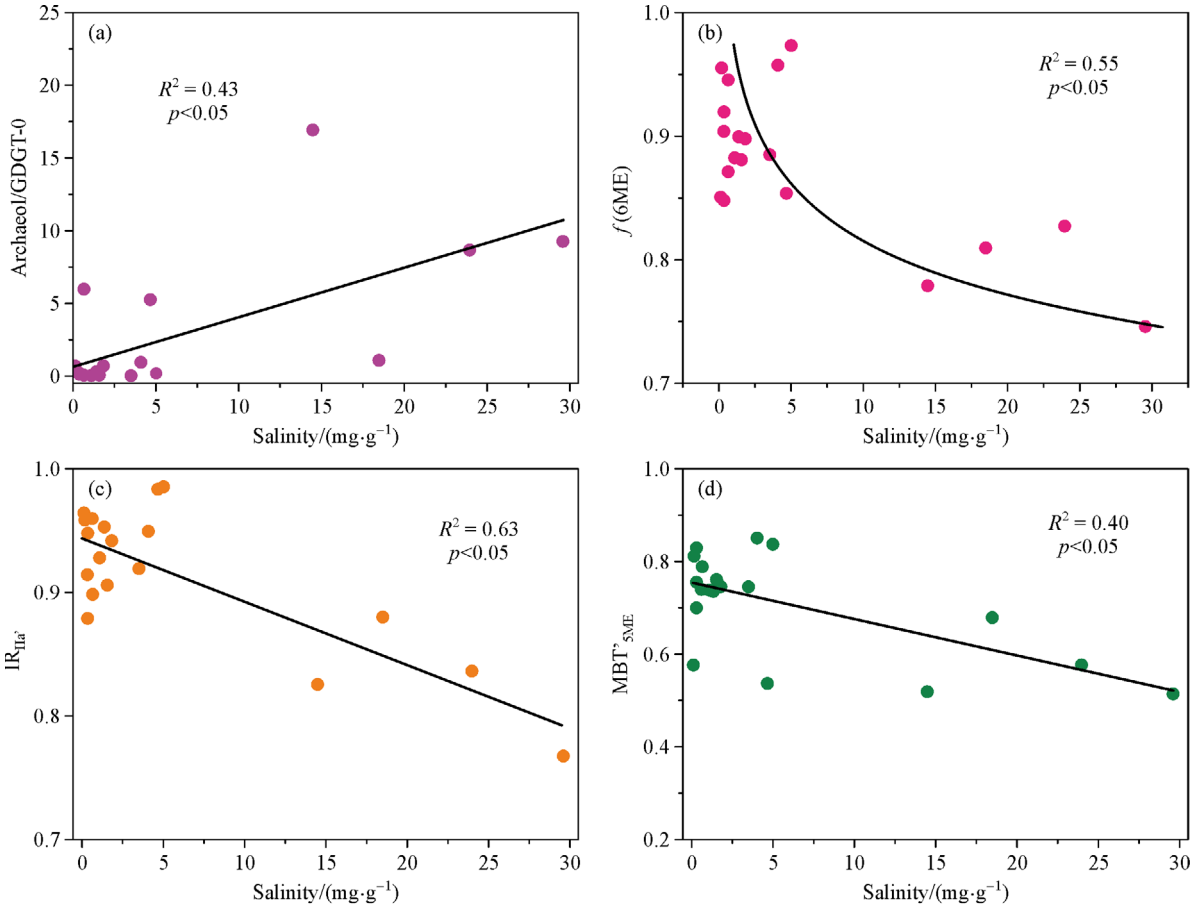

Fig. 10 Scatter plots showing relationship of (a) archaeol/GDGT-0, (b) *f*(6ME), (c) $IR_{IIa'}$, and (d) MBT'$_{5ME}$ with soil salinity.

Certain applications of these proxies to ancient sediments appear to overestimate temperatures; this was considered to be a bias toward the summer temperature, caused by the optimum growth of brGDGT-producing bacteria in the warm seasons (Peterse et al., 2011; Deng et al., 2016; Thomas et al., 2016). In our research, the three sites, with contrasting temperature seasonality albeit similar MAAT, provide a unique opportunity to assess whether these temperature proxies have a specific seasonal bias or not.

The MBT'$_{5ME}$ of the NY soils varies from 0.67 to 0.88 (average 0.82; Lei et al., 2016) and that of the KM soils ranges from 0.66 to 0.89 (average 0.79; Lei et al., 2016). In contrast, the MBT'$_{5ME}$ of the TRP soils varies between 0.51 and 0.85, which is consistently lower than those of the NY and KM soils. On the global scale, the MBT'$_{5ME}$ is primarily related to the MAAT (Fig. 8(c)), although certain additional factors, e.g. soil salinity, are likely to affect it. As the NY and KM soils are not subjected to salinization, four data points of TRP soils (with soil salinity > 10 mg/g) are excluded to minimize the influence of salinity on the comparison result. Without those four data points, the average MBT'$_{5ME}$ of the TRP soils (n = 15) is 0.74, corresponding to a MAAT estimate of 14.8°C; this value approaches the actual MAAT for the three sites. The average MAAT estimate based on the MBT'$_{5ME}$ values of NY and KM are 17.3°C and 16.1°C, respectively; both are marginally higher than that for TRP and their corresponding actual temperatures (Fig. 11(a)). At this stage, we can draw a conclusion that the MBT'$_{5ME}$ proxy-inferred temperature does not exhibit a significant bias toward the summer temperature because the MBT'$_{5ME}$ of the TRP soils would be significantly larger than those for the NY and KM soils if the seasonality exerts a significant impact on the temperature proxy.

In addition, there is also no significant bias toward the summer temperature in the $MAAT_{mr}$ proxy for the TRP soils. We compared the difference in the temperature estimates derived from the $MAAT_{mr}$ proxy for these three sites. The MAAT derived from the $MAAT_{mr}$ for the TRP soils (average 4.6°C) are significantly lower than those yielded by the MBT'$_{5ME}$ (Fig. 11(b)); however, the temperatures estimated from the $MAAT_{mr}$ of the NY and KM soils are close to the actual temperatures. This is because the global calibration of $MAAT_{mr}$ for temperature calculation is somewhat dependent on the fractional abundance of Ia. The fractional abundance of Ia in the TRP soils (0.07–0.16) is significantly lower than those in the NY (0.18–0.75) and KM (0.17–0.71) soils. Moreover,

Table 2 Fractional abundance of isoGDGTs and brGDGTs in the TRP soils. The fractional abundance of each isoGDGT component is based on only the isoGDGTs, whereas the fractional abundance of the brGDGTs is calculated relative to the total brGDGTs

Sample	f(GDGT-0)	f(GDGT-1)	f(GDGT-2)	f(GDGT-3)	f(Cren)	f(Cren')	f(IIIa)	f(IIIa')	f(IIIb)	f(IIIb')	f(IIa)	f(IIa')	f(IIb)	f(IIb')	f(IIc)	f(IIc')	f(Ia)	f(Ib)	f(Ic)
TLF-01	0.31	0.06	0.08	0.03	0.46	0.06	0.09	0.05	0.00	0.01	0.02	0.55	0.01	0.09	0.00	0.00	0.13	0.04	0.00
TLF-02	0.56	0.05	0.05	0.02	0.29	0.03	0.09	0.08	0.02	0.00	0.01	0.54	0.01	0.12	0.00	0.00	0.08	0.04	0.01
TLF-03	0.44	0.06	0.06	0.03	0.37	0.04	0.01	0.24	0.01	0.01	0.02	0.48	0.01	0.10	0.00	0.01	0.07	0.04	0.01
TLF-04	0.51	0.01	0.11	0.03	0.31	0.03	0.06	0.15	0.01	0.02	0.09	0.29	0.04	0.11	0.01	0.02	0.10	0.08	0.02
TLF-07	0.69	0.02	0.03	0.01	0.23	0.02	0.04	0.14	0.01	0.02	0.08	0.36	0.04	0.10	0.01	0.01	0.10	0.07	0.01
TLF-08	0.78	0.01	0.02	0.02	0.16	0.01	0.02	0.17	0.00	0.00	0.08	0.41	0.04	0.10	0.00	0.00	0.12	0.07	0.00
TLF-09	0.92	0.00	0.01	0.00	0.06	0.01	0.02	0.12	0.01	0.02	0.03	0.38	0.03	0.15	0.00	0.01	0.12	0.10	0.01
TLF-10	0.49	0.02	0.03	0.02	0.41	0.03	0.03	0.09	0.01	0.01	0.04	0.32	0.05	0.16	0.01	0.01	0.13	0.12	0.03
TLF-11	0.87	0.01	0.00	0.00	0.10	0.01	0.02	0.11	0.01	0.02	0.03	0.39	0.03	0.15	0.00	0.01	0.13	0.10	0.01
TLF-12	0.83	0.01	0.01	0.01	0.13	0.01	0.02	0.11	0.00	0.02	0.04	0.37	0.02	0.15	0.00	0.01	0.14	0.11	0.02
TLF-13	0.83	0.01	0.01	0.01	0.13	0.01	0.02	0.11	0.01	0.02	0.04	0.32	0.02	0.15	0.00	0.01	0.16	0.14	0.02
TLF-14	0.77	0.01	0.02	0.01	0.17	0.02	0.02	0.11	0.02	0.02	0.04	0.32	0.02	0.16	0.00	0.01	0.15	0.12	0.02
TLF-15	0.83	0.01	0.01	0.01	0.13	0.01	0.02	0.17	0.00	0.02	0.04	0.41	0.02	0.15	0.00	0.01	0.11	0.06	0.01
TLF-16	0.86	0.01	0.01	0.01	0.10	0.01	0.01	0.19	0.00	0.02	0.02	0.44	0.01	0.15	0.00	0.01	0.09	0.06	0.01
TLF-18	0.70	0.02	0.02	0.01	0.22	0.03	0.01	0.01	0.01	0.01	0.03	0.55	0.03	0.14	0.00	0.01	0.10	0.08	0.02
TLF-19	0.68	0.02	0.02	0.01	0.24	0.03	0.01	0.13	0.01	0.01	0.02	0.42	0.02	0.12	0.00	0.01	0.09	0.06	0.10
TLF-20	0.55	0.02	0.04	0.02	0.34	0.03	0.01	0.12	0.00	0.02	0.03	0.43	0.03	0.12	0.00	0.01	0.11	0.08	0.02
TLF-21	0.83	0.02	0.01	0.01	0.13	0.01	0.00	0.19	0.00	0.00	0.03	0.51	0.01	0.07	0.00	0.00	0.14	0.05	0.00
TLF-22	0.69	0.02	0.02	0.01	0.25	0.01	0.01	0.24	0.01	0.00	0.01	0.56	0.00	0.07	0.00	0.00	0.07	0.02	0.00

Table 3 Environmental variables and proxies for the TRP soils (n = 19)

Sample	pH	SWC	Salinity/ ($mg \cdot g^{-1}$)	Archaeol/ GDGT – 0	GDGT-0/Cren	BIT	$IR_{IIIa'}$	$IR_{IIa'}$	MBT	MBT'	MBT'$_{5ME}$	MBT'$_{6ME}$	CBT	CBT$_{5ME}$	CBT$_{6ME}$	f(5ME)	f(6ME)	$R_{i/b}$	MAAT[a)]	MAAT$_{mr}$[b)]
TLF-01	7.81	25.43	0.15	0.74	0.66	0.78	0.36	0.96	0.17	0.17	0.58	0.19	0.70	0.48	0.72	0.15	0.85	0.50	9.6	3.8
TLF-02	7.99	0.16	4.69	5.27	1.94	0.89	0.46	0.98	0.13	0.13	0.54	0.15	0.57	0.29	0.59	0.15	0.85	0.35	8.3	3.6
TLF-03	8.18	0.23	0.65	5.99	1.18	0.86	0.96	0.96	0.12	0.12	0.74	0.12	0.60	0.28	0.62	0.05	0.95	0.37	14.7	3.1
TLF-04	8.04	0.38	29.57	9.27	1.67	0.82	0.71	0.77	0.21	0.21	0.51	0.26	0.32	0.21	0.32	0.25	0.75	0.50	7.6	3.3
TLF-07	8.01	0.00	14.48	16.93	3.03	0.85	0.76	0.83	0.18	0.19	0.52	0.23	0.40	0.21	0.43	0.22	0.78	0.56	7.8	3.0
TLF-08	7.96	0.00	23.95	8.68	4.83	0.68	0.89	0.84	0.19	0.19	0.58	0.22	0.48	0.27	0.51	0.17	0.83	2.31	9.6	2.7
TLF-09	7.74	0.20	3.53	0.04	14.72	0.57	0.86	0.92	0.24	0.24	0.75	0.27	0.27	0.07	0.28	0.12	0.88	8.14	14.9	5.5
TLF-10	7.58	0.41	18.49	1.11	1.17	0.66	0.71	0.88	0.28	0.28	0.68	0.32	0.17	0.00	0.19	0.19	0.81	0.74	12.8	6.2
TLF-11	7.61	0.36	1.11	0.06	8.58	0.57	0.84	0.93	0.24	0.24	0.74	0.26	0.30	0.08	0.32	0.12	0.88	4.93	14.6	5.4
TLF-12	7.81	5.22	1.58	0.07	6.48	0.63	0.86	0.91	0.27	0.27	0.76	0.30	0.29	0.13	0.30	0.12	0.88	3.01	15.3	5.9
TLF-13	7.87	0.20	0.68	0.06	6.33	0.58	0.84	0.90	0.31	0.32	0.79	0.35	0.22	0.08	0.22	0.13	0.87	3.56	16.2	7.0
TLF-14	7.84	0.69	0.35	0.05	4.52	0.54	0.84	0.88	0.28	0.29	0.75	0.32	0.23	0.13	0.23	0.15	0.85	3.21	15.2	6.1
TLF-15	7.88	8.88	0.35	0.08	6.13	0.55	0.89	0.91	0.18	0.18	0.70	0.20	0.40	0.29	0.40	0.10	0.90	4.44	13.4	3.7
TLF-16	7.92	1.49	0.21	0.13	8.23	0.63	0.97	0.96	0.14	0.16	0.81	0.17	0.40	0.16	0.40	0.04	0.96	3.53	16.9	4.1
TLF-18	7.98	0.53	1.40	0.30	3.19	0.76	0.51	0.95	0.19	0.20	0.74	0.21	0.43	0.06	0.47	0.10	0.90	0.98	14.6	4.7
TLF-19	7.86	0.00	0.36	0.28	2.84	0.74	0.94	0.95	0.25	0.26	0.83	0.27	0.42	0.16	0.45	0.08	0.92	0.99	17.5	7.0
TLF-20	7.51	0.10	1.84	0.70	1.60	0.61	0.91	0.94	0.22	0.22	0.75	0.24	0.38	0.08	0.42	0.10	0.90	1.28	14.9	5.3
TLF-21	7.17	0.00	4.09	0.96	6.29	0.74	1.00	0.95	0.19	0.19	0.85	0.20	0.71	0.43	0.72	0.04	0.96	2.29	18.2	4.2
TLF-22	7.59	0.35	5.02	0.19	2.79	0.73	0.98	0.99	0.09	0.09	0.84	0.09	0.82	0.48	0.83	0.03	0.97	1.32	17.7	2.7
Average	7.81	2.35	5.92	2.68	4.54	0.70	0.80	0.92	0.20	0.21	0.71	0.23	0.43	0.21	0.44	0.12	0.88	2.26	13.7	4.6
Standard deviation	±0.23	±6.02	±8.88	±4.59	±3.48	±0.11	±0.18	±0.06	±0.06	±0.06	±0.11	±0.07	±0.18	±0.14	±0.18	±0.06	±0.06	±2.04	±3.45	±1.42

a) MAAT and b) MAAT$_{mr}$ calculated according to the global calibration of MBT'$_{5ME}$ (Eq. (11)) and the global calibration based on the multiple linear regression (Eq. (12)) reported by De Jonge et al. (2014a).

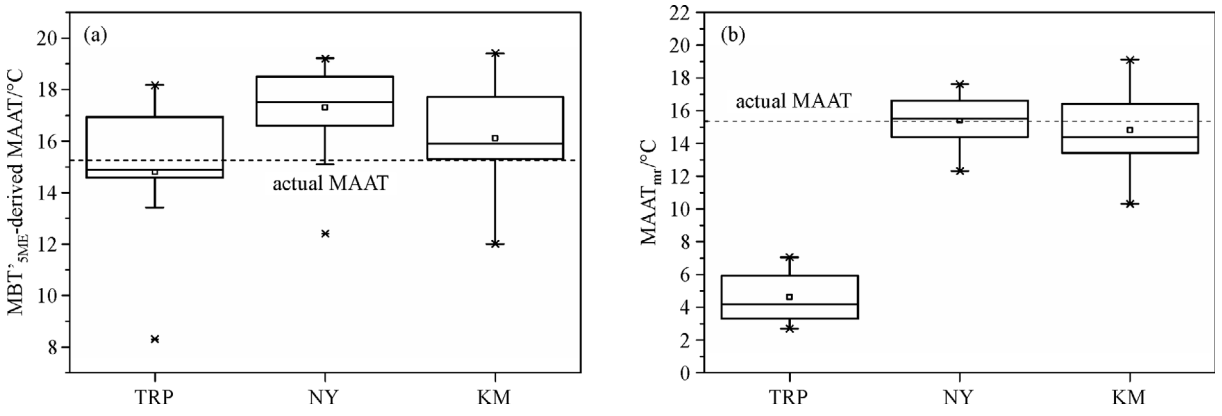

Fig. 11 (a) Box plots of MAAT estimates for the TRP, NY, and KM soils, calculated using the global calibration of MBT'$_{5ME}$ (De Jonge et al., 2014a). It displays the minimum, maximum, median, lower quartile (25%), and upper quartile (75%) information for the MAAT; (b) Box plots of MAAT$_{mr}$ estimates for the TRP, NY, and KM soils, produced using multiple linear regression calibration (Eq. (11)). The MAAT$_{mr}$ estimates for the TRP soils are significantly lower than those for the NY and KM soils.

as stated in the previous sections, the distributions of these nine brGDGTs are remarkably different from those in other places. Therefore, it is likely that the MAAT$_{mr}$ is not applicable to TRP as this calibration is developed according to a soil dataset with a completely different brGDGT distribution pattern. Moreover, the abundance of Ia appears to decrease with increase in soil aridity (Dang et al., 2016). It is reasonable to observe a significantly lower Ia abundance in the dry TRP soils. The global calibration of MAAT$_{mr}$ was also observed to underestimate the temperature in a loess-paleosol sequence during the arid late Holocene (Tang et al., 2017). This collectively indicates that a MAAT$_{mr}$ proxy is likely to be affected by the soil moisture and should not be applied in arid regions.

4 Conclusions

The GDGTs in the TRP soils exhibit a distributional pattern that is typical for semi-arid and arid regions: isoGDGTs dominate over brGDGTs, and 6-methyl brGDGTs, particularly IIa', are the major brGDGT components. The unusually high GDGT-0/crenarchaeol ratio in the arid TRP soils cannot be attributed to the dominance of methanogenic archaea or MCG in the archaeal community, where halophilic archaea are generally the most abundant. BrGDGT proxies including *f*(6-ME), IR$_{IIa'}$, and MBT'$_{5ME}$, were all to an extent affected by soil salinity. A comparison of the MBT'$_{5ME}$-inferred temperature of the TRP, NY, and KM soils reveals no significant bias toward summer temperature in the brGDGT paleo-thermometer for MBT'$_{5ME}$.

Acknowledgements We sincerely thank four anonymous reviewers for their constructive comments, which improved the quality of our original manuscript. The work was sponsored by the National Natural Science Foundation of China (Grant No. 41602189), the project of 'Cradle Plan', China University of Geosciences, Wuhan (No. CUGL170403). We also thank Chao GAO and Yue LI for assistance with experiments and Shijin ZHAO for sample analysis.

References

Auguet J C, Barberan A, Casamayor E O (2010). Global ecological patterns in uncultured Archaea. ISME J, 4(2): 182–190

Balsam W L, Ellwood B B, Ji J F, Williams E R, Long X Y, El Hassani A (2011). Magnetic susceptibility as a proxy for rainfall: worldwide data from tropical and temperate climate. Quat Sci Rev, 30(19 – 20): 2732–2744

Besseling M A, Hopmans E C, Boschman R C, Sinninghe Damsté J S, Villanueva L (2018). Benthic Archaea as potential sources of tetraether membrane lipids in sediments across an oxygen minimum zone. Biogeosci, 15(13): 4047–4064

Blaga C I, Reichart G J, Heiri O, Sinninghe Damsté J S (2009). Tetraether membrane lipid distributions in water-column particulate matter and sediments: a study of 47 European lakes along a north–south transect. J Paleolimnol, 41(3): 523–540

Brassell S C, Eglinton G, Marlowe I T, Pflaumann U, Sarnthein M (1986). Molecular stratigraphy: a new tool for climatic assessment. Nature, 320(6058): 129–133

Dang X Y, Yang H, Naafs B D A, Pancost R D, Xie S C (2016). Evidence of moisture control on the methylation of branched glycerol dialkyl glycerol tetraethers in semi-arid and arid soils. Geochim Cosmochim Acta, 189: 24–36

De Jonge C, Hopmans E C, Stadnitskaia A, Rijpstra W I C, Hofland R, Tegelaar E, Sinninghe Damsté J S (2013). Identification of novel penta- and hexamethylated branched glycerol dialkyl glycerol tetraethers in peat using HPLC–MS^2, GC–MS and GC–SMB-MS. Org Geochem, 54(1): 78–82

De Jonge C, Hopmans E C, Zell C I, Kim J H, Schouten S, Sinninghe Damsté J S (2014a). Occurrence and abundance of 6-methyl branched glycerol dialkyl glycerol tetraethers in soils: implications for palaeoclimate reconstruction. Geochim Cosmochim Acta, 141: 97–112

De Jonge C, Stadnitskaia A, Hopmans E C, Cherkashov G, Fedotov A,

Sinninghe Damsté J S (2014b). In situ produced branched glycerol dialkyl glycerol tetraethers in suspended particulate matter from the Yenisei River, Eastern Siberia. Geochim Cosmochim Acta, 125(1): 476–491

Deng L H, Jia G D, Jin C F, Li S J (2016). Warm season bias of branched GDGT temperature estimates causes underestimation of altitudinal lapse rate. Org Geochem, 96: 11–17

Elling F J, Könneke M, Nicol G W, Stieglmeier M, Bayer B, Spieck E, de la Torre J R, Becker K W, Thomm M, Prosser J I, Herndl G J, Schleper C, Hinrichs K U (2017). Chemotaxonomic characterisation of the thaumarchaeal lipidome. Environ Microbiol, 19(7): 2681–2700

Heller F, Liu T S (1982). Magnetostratigraphical dating of loess deposits in China. Nature, 300(5891): 431–433

Hopmans E C, Weijers J W H, Schefuß E, Herfort L, Sinninghe Damsté J S, Schouten S (2004). A novel proxy for terrestrial organic matter in sediments based on branched and isoprenoid tetraether lipids. Earth Planet Sci Lett, 224(1–2): 107–116

Huang X Y, Meyers P A, Xue J T, Gong L F, Wang X X, Xie S C (2015). Environmental factors affecting the low temperature isomerization of homohopanes in acidic peat deposits, central China. Geochim Cosmochim Acta, 154(7): 212–228

Huguet C, Hopmans E C, Febo-Ayala W, Thompson D H, Sinninghe Damsté J S, Schouten S (2006). An improved method to determine the absolute abundance of glycerol dibiphytanyl glycerol tetraether lipids. Org Geochem, 37(9): 1036–1041

Jiang H C, Mao X, Xu H Y, Thompson J, Wang P, Ma X L (2011). Last glacial pollen record from Lanzhou (Northwestern China) and possible forcing mechanisms for the MIS 3 climate change in Middle to East Asia. Quat Sci Rev, 30(5 – 6): 769–781

Kang S C, Wang F Y, Morgenstern U, Zhang Y L, Grigholm B, Kaspari S, Schwikowski M, Ren J W, Yao T D, Qin D H, Mayewski P A (2015). Dramatic loss of glacier accumulation area on the Tibetan Plateau revealed by ice core tritium and mercury records. Cryosphere, 9(3): 1213–1222

Kemp D B, Robinson S A, Crame J A, Francis J E, Ineson J, Whittle R J, Bowman V, O'Brien C (2014). A cool temperate climate on the Antarctic Peninsula through the latest Cretaceous to early Paleogene. Geology, 42(7): 583–586

Lei Y Y, Yang H, Dang X Y, Zhao S J, Xie S C (2016). Absence of a significant bias towards summer temperature in branched tetraether-based paleothermometer at two soil sites with contrasting temperature seasonality. Org Geochem, 94: 83–94

Leng M J, Marshall J D (2004). Palaeoclimate interpretation of stable isotope data from lake sediment archives. Quat Sci Rev, 23(7–8): 811–831

Lu H Y, Wu N Q, Yang X D, Jiang H, Liu K B, Liu T S (2006). Phytoliths as quantitative indicators for the reconstruction of past environmental conditions in China. I: Phytolith-based transfer functions. Quat Sci Rev, 25(9–10): 945–959

Menges J, Huguet C, Alcañiz J M, Fietz S, Sachse D, Rosell-Melé A (2014). Influence of water availability in the distributions of branched glycerol dialkyl glycerol tetraether in soils of the Iberian Peninsula. Biogeosciences, 11(10): 2571–2581

Miranda M C C, Rossetti D F, Pessenda L C R (2009). Quaternary paleoenvironments and relative sea-level changes in Marajó Island (Northern Brazil): facies, $\delta^{13}C$, $\delta^{15}N$ and C/N. Palaeogeogr Palaeoclimatol Palaeoecol, 282(4): 19–31

Pancost R D, McClymont E L, Bingham E M, Roberts Z, Charman D J, Hornibrook E R, Blundell A, Chambers F M, Lim K L, Evershed R P (2011). Archaeol as a methanogen biomarker in ombrotrophic bogs. Org Geochem, 42(10): 1279–1287

Pancost R D, Taylor K W R, Inglis G N, Kennedy E M, Handley L, Hollis C J, Crouch E M, Pross J, Huber M, Schouten S, Pearson P N, Morgans H E G, Raine J I (2013). Early Paleogene evolution of terrestrial climate in the SW Pacific, Southern New Zealand. Geochem Geophys Geosyst, 14(12): 5413–5429

Pearson A, Huang Z, Ingalls A E, Romanek C S, Wiegel J, Freeman K H, Smittenberg R H, Zhang C L (2004). Nonmarine crenarchaeol in Nevada hot springs. Appl Environ Microbiol, 70(9): 5229–5237

Pearson A, Pi Y D, Zhao W D, Li W J, Li Y L, Inskeep W, Perevalova A, Romanek C, Li S G, Zhang C L (2008). Factors controlling the distribution of archaeal tetraethers in terrestrial hot springs. Appl Environ Microbiol, 74(11): 3523–3532

Pendall E, Markgraf V, White J W C, Dreier M, Kenny R (2001). Multiproxy record of Late Pleistocene Holocene climate and vegetation changes from a peat bog in Patagonia. Quat Res, 55(2): 168–178

Peterse F, Prins M A, Beets C J, Troelstra S R, Zheng H B, Gu Z Y, Schouten S, Sinninghe Damsté J S (2011). Decoupled warming and monsoon precipitation in East Asia over the last deglaciation. Earth Planet Sci Lett, 301(1–2): 256–264

Peterse F, van der Meer J, Schouten S, Weijers J W H, Fierer N, Jackson R B, Kim J H, Sinninghe Damsté J S (2012). Revised calibration of the MBT–CBT paleotemperature proxy based on branched tetraether membrane lipids in surface soils. Geochim Cosmochim Acta, 96(11): 215–229

Schouten S, Hopmans E C, Sinninghe Damsté J S (2013). The organic geochemistry of glycerol dialkyl glycerol tetraether lipids: a review. Org Geochem, 54(1): 19–61

Sinninghe Damsté J S, Ossebaar J, Schouten S, Verschuren D (2012). Distribution of tetraether lipids in the 25-ka sedimentary record of Lake Challa: extracting reliable TEX_{86} and MBT/CBT palaeotemperatures from an equatorial African lake. Quat Sci Rev, 50(6): 43–54

Sinninghe Damsté J S, Rijpstra W I, Hopmans E C, Foesel B U, Wust P K, Overmann J, Tank M, Bryant D A, Dunfield P F, Houghton K, Stott M B (2014). Ether- and ester-bound iso-diabolic acid and other lipids in members of acidobacteria subdivision 4. Appl Environ Microbiol, 80(17): 5207–5218

Tang C Y, Yang H, Dang X Y, Xie S C (2017). Comparison of paleotemperature reconstructions using microbial tetraether thermometers of the Chinese loess-paleosol sequence for the past 350000 years. Sci China Earth Sci, 60(6): 1159–1170

ter Braak C J F, Smilauer P (2002). CANOCO Reference Manual and CanoDraw for Windows User's Guide: Software for Canonical Community Ordination (version 4.5). Ithaca, NY, USA. 500

Thomas E K, Clemens S C, Sun Y B, Prell W L, Huang Y S, Gao L, Loomis S, Chen G S, Liu Z Y (2016). Heterodynes dominate precipitation isotopes in the East Asian monsoon region, reflecting interaction of multiple climate factors. Earth Planet Sci Lett, 455: 196–206

Thornton S F, McManus J (1994). Application of organic carbon and

nitrogen stable isotope and C/N Ratios as source indicators of organic matter provenance in estuarine systems: evidence from the Tay Estuary, Scotland. Estuar Coast Shelf Sci, 38(3): 219–233

Újvári G, Kok J F, Varga G, Kovács J (2016). The physics of wind-blown loess: implications for grain size proxy interpretations in Quaternary paleoclimate studies. Earth Sci Rev, 154: 247–278

Valenzuela-Encinas C, Neria-González I, Alcántara-Hernández R, Enríquez-Aragón J, Estrada-Alvarado I, Hernández-Rodríguez C, Dendooven L, Marsch R (2008). Phylogenetic analysis of the archaeal community in an alkaline-saline soil of the former lake Texcoco (Mexico). Extremophiles, 12(2): 247–254

Wang H Y, Liu W G, Lu H X (2016). Appraisal of branched glycerol dialkyl glycerol tetraether-based indices for North China. Org Geochem, 98: 118–130

Wang H Y, Liu W G, Zhang C L (2014). Dependence of the cyclization of branched tetraethers on soil moisture in alkaline soils from arid-subhumid China: implications for palaeorainfall reconstructions on the Chinese Loess Plateau. Biogeosciences, 11(23): 6755–6768

Wang H Y, Liu W G, Zhang C L, Jiang H C, Dong H L, Lu H X, Wang J X (2013). Assessing the ratio of archaeol to caldarchaeol as a salinity proxy in highland lakes on the northeastern Qinghai-Tibetan Plateau. Org Geochem, 54: 69–77

Wang Y J, Cheng H, Edwards R L, Kong X G, Shao X H, Chen S T, Wu J Y, Jiang X Y, Wang X F, An Z S (2008). Millennial- and orbital-scale changes in the East Asian monsoon over the past 224,000 years. Nature, 451(7182): 1090–1093

Weijers J W H, Schouten S, Hopmans E C, Geenevasen J A J, David O R P, Coleman J M, Pancost R D, Sinninghe Damste J S (2006a). Membrane lipids of mesophilic anaerobic bacteria thriving in peats have typical archaeal traits. Environ Microbiol, 8(4): 648–657

Weijers J W H, Schouten S, Spaargaren O C, Sinninghe Damsté J S (2006b). Occurrence and distribution of tetraether membrane lipids in soils: implications for the use of the TEX_{86} proxy and the BIT index. Org Geochem, 37(12): 1680–1693

Weijers J W H, Schouten S, van den Donker J C, Hopmans E C, Sinninghe Damsté J S (2007). Environmental controls on bacterial tetraether membrane lipid distribution in soils. Geochim Cosmochim Acta, 71(3): 703–713

Willard D A, Weimer L M, Riegel W L (2001). Pollen assemblages as paleoenvironmental proxies in the Florida Everglades. Rev Palaeobot Palynol, 113(4): 213–235

Wu F L, Fang X M, Ma Y Z, Herrmann M, Mosbrugger V, An Z, Miao Y (2007). Plio–Quaternary stepwise drying of Asia: evidence from a 3-Ma pollen record from the Chinese Loess Plateau. Earth Planet Sci Lett, 257(1–2): 160–169

Xie S C, Pancost R D, Chen L, Evershed R P, Yang H, Zhang K X, Huang J H, Xu Y D (2012). Microbial lipid records of highly alkaline deposits and enhanced aridity associated with significant uplift of the Tibetan Plateau in the Late Miocene. Geology, 40(4): 291–294

Yang H, Lü X X, Ding W H, Lei Y Y, Dang X Y, Xie S C (2015a). The 6-methyl branched tetraethers significantly affect the performance of the methylation index (MBT') in soils from an altitudinal transect at Mount Shennongjia. Org Geochem, 82: 42–53

Yang H, Pancost R D, Dang X Y, Zhou X Y, Evershed R P, Xiao G Q, Tang C Y, Gao L, Guo Z T, Xie S C (2014). Correlations between microbial tetraether lipids and environmental variables in Chinese soils: optimizing the paleo-reconstructions in semi-arid and arid regions. Geochim Cosmochim Acta, 126: 49–69

Yang H, Pancost R D, Jia C L, Xie S C (2016). The response of archaeal tetraether membrane lipids in surface soils to temperature: a potential paleothermometer in paleosols. Geomicrobiol J, 33(2): 98–109

Yang H, Xiao W J, Jia C L, Xie S (2015b). Paleoaltimetry proxies based on bacterial branched tetraether membrane lipids in soils. Front Earth Sci, 9(1): 13–25

Zielinski U, Gersonde R (1997). Diatom distribution in Southern Ocean surface sediments (Atlantic sector): implications for paleoenvironmental reconstructions. Palaeogeogr Palaeoclimatol Palaeoecol, 129 (3–4): 213–250